International Journal of Scientific & Engineering Research, Volume 6, Issue 1, January-2015
ISSN 2229-5518

Anomaly in Elastic properties of Rutile TiO_2 and tetragonal $BaTiO_3$

Ghous Narejo

Abstract

First-principles computational techniques are employed on Rutile TiO_2 and tetragonal $BaTiO_3$. The computations done for the second-order elastic constants (SOEC) and equations of state. The bulk modulus is computed by two independent methods and compared with experiment. A variety of potentials and basis sets are used. The impact on the computational values due to the potentials, basis sets, and the crystalline geometry optimization is discussed. A novel computational formalism is employed to extract the anomaly in the elastic properties of tetragonal $BaTiO_3$.

Keywords: Elastic constant, Bulk modulus

The article is subdivided into two major sections. The first section employs the ab-initio and DFT computational algorithms to compute the elastic constants and bulk moduli of rutile $TiO2$ crystal. In the second section,the prior results on Rutile $TiO2$ are utilized to expose the complexity in computations that are carried out on tetragonal $BaTiO3$.

1. Part I: Computations On Rutile TiO_2

Titanium dioxide (TiO_2) is an important transition metal oxide, which exists in anatase, rutile and brookite phases [1]. There is a considerable interest in the fabrication [2] of this material. It is employed extensively in semiconductors, optical devices, photovoltaic cells, gas sensors, and electrochemical storage devices [3].

Due to its technological importance, the crystalline structure and properties of rutile TiO_2 phases has remained a major focus of researchers [1, 4, 5]. The *ab-initio* Hartree Fock (HF) and density functional theory (DFT) techniques are employed by various research groups to compute the optimized electronic structure, band gap and charge density of rutile TiO_2 [6, 7, 1, 8].

The *ab-initio* computation of the elastic constants and bulk moduli of rutile TiO_2 are presented in this work using the CRYSTAL09 code [9]. The availability of precise and accurate values of experimental lattice parameters, elastic properties [10] and chemical bonding [11] has provided a considerable challenge to the reliability of *ab-initio* computational codes. Computational codes based upon the linear combination of atomic orbitals (LCAO) and plane waves (PW) were employed by refs. [6, 7, 1, 8, 5] to compute the optimized crystalline structure of rutile TiO_2. However, the inadequacy of the existing potentials [1, 7, 12, 6] to accurately predict the physics of TiO_2 has motivated a detailed analysis of a wide range of existing and new potentials [12, 6] The research on the structural and electronic properties has confirmed the relative accuracy of the hybrid potentials [12, 6, 7, 1, 6].

It is our view that there has been no systematic effort to explore the elastic properties of rutile TiO_2 using the LCAO code CRYSTAL09 [9]. CRYSTAL09 possesses a combination of geometry optimization techniques, basis sets, potentials and algorithms such as ELASTCON [9] (for second-order elastic constants) and EOS (equation of state) [9]. The experimental values of lattice parameters, elastic constants and bulk moduli [10] of TiO_2 rutile phase provided us an opportunity to confirm the relative merit of the ELASTCON and EOS programs [13**?**].

1.1. Computational procedure

We employed two different basis set combinations and a variety of potentials to compute the optimized lattice constants and elastic properties (see section 1.2 for the discussion of potentials and basis sets). The ELASTCON [9] and EOS [9] algorithms are employed to compute the elastic constants and bulk moduli of rutile TiO_2 in an automated manner. (See Fig. {tio for reference)

The two basis sets employed in computations are named as basis set 1 and 2 (see section 1.2 for basis set definitions). Optimized lattice parameters are computed with HF, DFT and hybrid potentials using the two unique basis sets. The computations of elastic constants and bulk moduli are performed by employing the ELASTCON algorithm [9]. The computations of bulk moduli are carried out by the EOS algorithm. Finally, the bulk moduli obtained with ELASTCON and EOS algorithms are compared. Optimized lattice parameters, elastic constants and bulk moduli, obtained with basis set 1 and 2, are also compared with the experimental values where possible.

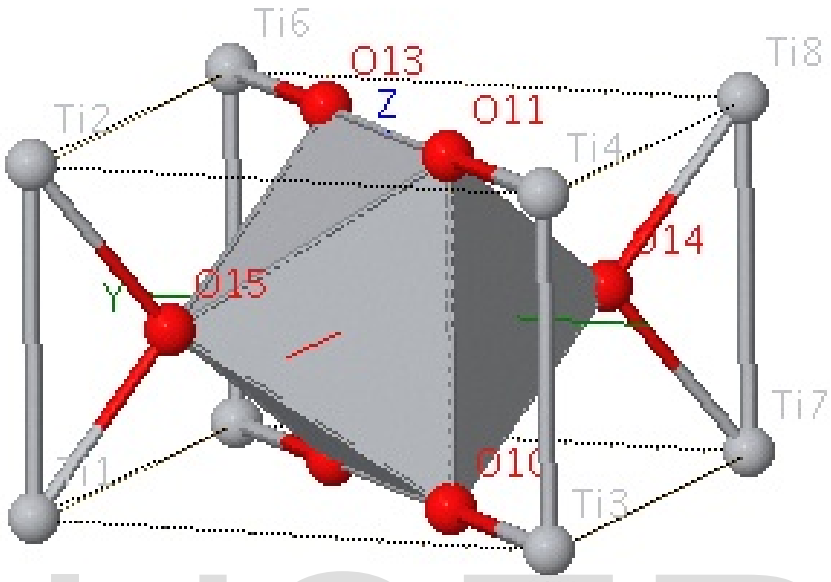

Figure 1: The Unit Cell of Rutile TiO2.

A possible contribution of this research work is to assist a general reader in understanding the complex dependance of the elastic properties on the quality of basis sets, potentials, SCF process, ELASTCON and EOS parameters. Experimental values of lattice parameters, elastic constants and bulk moduli of rutile TiO_2 are provide an additional assistance to a researcher in adequate implementation of ELASTCON and EOS programs.

A significant number of computations and experiments are conducted on rutile TiO_2. It is also noticed that a high precision has been achieved in the experimental lattice parameters of rutile TiO_2 [14]. The availability of the experimental values of lattice constants, elastic constants and bulk moduli of rutile TiO_2, provides a highly valuable resource to conduct new research. In contrast, computations of elastic constants and bulk moduli have been done in an isolated and non-systematic manner.

A vast majority of *ab-initio* computations have already tried DFT exchange and correlation potentials [7, 15, 1]. The need of hybrid potentials arose because HF [12] underestimated and DFT potentials overestimated the lattice parameters of rutile TiO_2. It has been found that the higher exchange and correlation associated with the transition metals requires new

hybrid potentials with variable exchange and correlation [7, 15, 1]. The HF, DFT as well as hybrid potentials are employed in this work [9] to fill the gap with regard to the efficient, accurate and systematic computations of elastic properties of rutile TiO_2.

1.2. Potentials and basis sets

The HF, local and non-local DFT potentials have consistently resulted in inadequate results of the lattice parameters. The first principles computations done with PW codes [16, 17, 18, 19, 20, 21] can not employ the hybrid mixing of HF exchange and DFT correlations.

Therefore, we employed hybrid potentials in our computations of elastic properties as suggested in refs. [12, 6, 1, 7, 15]. The hybridization between the Ti d-orbitals and O p-orbitals requires that an adequate percentage of exchange and correlation is introduced in the potential while computing the electronic structure of a material [22]. The DFT-PWGGA and DFT-PBE potentials lack the exchange part and HF lacks the correlation part barring them from being as accurate as hybrid potentials.

In addition to using hybrid potentials, the proper choice of basis sets, SCF tolerances, ELASTCON and EOS parameters can achieve the optimum efficiency as well as accuracy (see sections 1.5 and 1.7). Moreover, great care must be taken to employ adequate SCF tolerances consistently.

Additionally, we selected the O-8411d1[23] and O-6311d1 basis sets for O atoms and defined these basis sets as basis set 1 and 2, respectively. Both basis sets used a pseudopotential basis set for the Ti atom [9]. The aim of employing these combinations was to separate the basis set dependency from other factors such as potentials, SCF parameters, ELASTCON and EOS tolerances.

The purpose of selecting basis set 1 and 2 is to understand the role of a basis set in combination with each individual potential. For basis set 1 and 2, the computations of lattice parameters, elastic constants and bulk moduli are performed with a specific purpose to assist a general reader.

The sensitivity of of the elastic properties with respect to deviations in the lattice parameters [1] suggests that a detailed set of potentials must be employed to compute the lattice parameters and understand their influences on the elastic constant values. The impact of a particular potential and basis set on the computational values of lattice parameters, elastic constants and bulk moduli values can be understood by careful comparisons of results achieved for a variety of these basis sets and potentials. Further, we have

also performed comparisons of our computational results for each potential and basis set combination with the refs. [1, 15, 7] to confirm their research findings. (See Fig. 2)

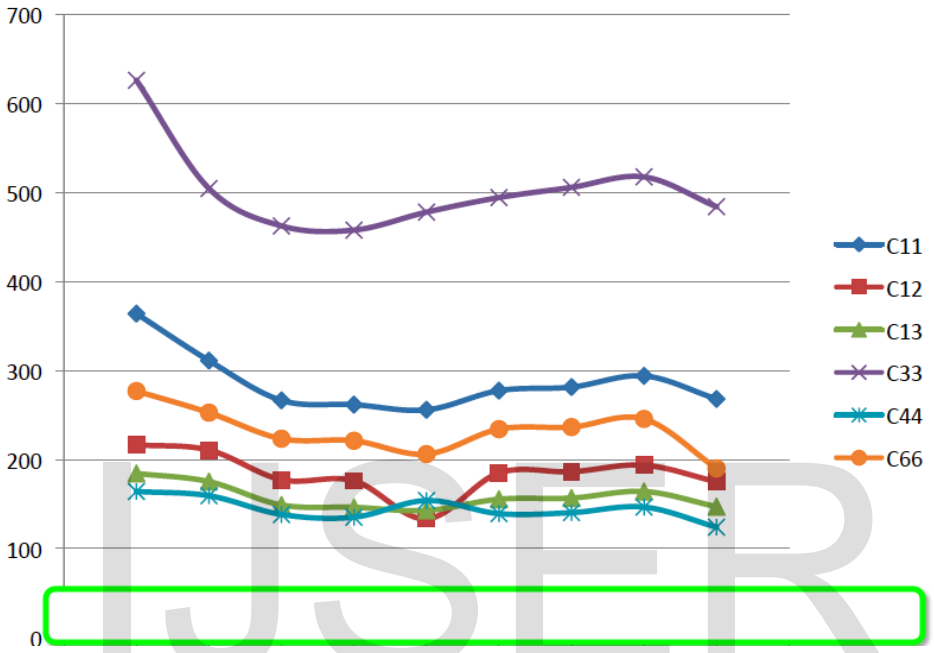

Figure 2: The elastic constants for Rutile TiO2.

1.3. Computational algorithms

1.4. ELASTCON

The computation of elastic constants and the bulk moduli is an automated procedure within the ELASTCON algorithm. The computational process begins with determining the crystalline symmetry of rutile TiO_2. An adequate number of strains must be applied to exploit the available symmetry in the crystalline structure under consideration. The analytic first derivative and the numerical second derivative of the total energy are carried out for each specific strain. Levenberg Marquardt (LM) curve fitting [24] is used to compute the required elastic constants for the rutile TiO_2 symmetry. The elastic constants can be extracted from the second derivative of the total energy as :

$$C_{\alpha\beta} = \frac{1}{V}\frac{\partial^2 E}{\partial\epsilon_\alpha \partial\epsilon_\beta}\bigg|_0. \tag{1}$$

In Eq. (1), the terms $C_{\alpha\beta}$, E, and V express the elastic constant tensor, energy and volume of the crystalline structure respectively.

The *ab-initio* computations are achieved by calculating the analytic first derivative and numerical second derivative of the total energy with respect to the applied strain. The appropriate number of strains are applied in a systematic manner, the elastic constants are calculated, and the compliance coefficients are computed from Eq. (3). The compliance coefficients are then utilized for the computation of the bulk modulus as shown in Eq. (2).

$$[S] = [C]^{-1} \tag{2}$$

$$B = 1/(S_{11} + S_{22} + S_{33} + 2(S_{12} + S_{13} + S_{23})). \tag{3}$$

The terms S_{ij} and B in Eq. (3) express the compliance tensor elements and bulk modulus, respectively.

1.4.1. EOS

The EOS algorithm employs changes [13] in the optimized volume of the rutile TiO_2 in a systematic manner. Additionally, the EOS algorithm allows the user to select a range of volumes and a number of the volumes within that range. For each of the volumes in the range, the CRYSTAL09 optimizes the internal co-ordinates and lattice parameters while keeping the volume constant. The energy vs. volume results are then curve-fitted to an EOS such as the Murnaghan EOS [25] shown in Eq. (4) (see ref. [13] for the CVOLOPT option employed during the constant volume geometry optimization for EOS computations).

The EOS algorithm in CRYSTAL09 contains a diversity of equations of state such as Birch Murnaghan, 3rd-order Birch Murnaghan, logarithmic, Vinet and polynomial. The 3rd-order Birch Murnaghan equation of state algorithm utilized for computing the bulk moduli from the energy vs. volume computations for rutile TiO_2 is :

$$E(V) = B_o V_o \left[\frac{1}{B'(B'-1)} \left(\frac{V_o}{V} \right)^{B'-1} + \frac{V}{B'V_o} - \frac{1}{B'-1} \right] + E_o. \tag{4}$$

In Eq. (4), V_0 represents the volume at the minimum energy, B_0 is the bulk modulus at pressure $P = 0$, $B^{'}$ is the derivative of the bulk modulus at $P = 0$ and E_0 is the minimum energy. The bulk modulus results are obtained with Levenberg-Marquardt curve fitting of the E vs. V computations. The detailed discussion about the ELASTCON [9] and EOS [9] algorithms can be seen in refs. [**?** 13].

1.5. Experiments

Due to its technological importance, a significant number of experiments have been conducted on rutile TiO_2 [26, 21, 10]. The experimental results of the electronic structure, band gap, optic and elastic properties are available of rutile TiO_2. The lattice parameters of the rutile TiO_2 have been determined [14] precisely up to the fifth significant figure. In addition, the pressure and temperature dependence of elastic constants and bulk moduli have also been explored through experimental means.

The experimental and computational values of elastic constants and bulk moduli [10] of rutile TiO_2 have special significance as they serve the purpose of linking these vital branches of research. The importance of achieving a consistency in the lattice parameters of rutile TiO_2 among diverse experimental techniques and computational codes is a remarkable achievement which is repeatedly observed by refs.[6, 7, 1, 15].

However, there are deviations in the experimental values of elastic constants and bulk moduli due to their dependence on the experimental details, pressure and temperature conditions [27]. Therefore, the sources that cause the variations in the experimental values[28, 27, 10, 29] must also be considered. However, the dependence of the experimental results on the nature of the experimental set up and ambient conditions can be explored and understood by robust and reliable *ab-initio* computational methods.

Fortunately, a detailed research is carried out by ref. [30] on variations in experimental and computational values of elastic constants and bulk moduli of rutile TiO_2. The elastic properties are changed by the change in the temperature and pressure conditions.

An increase in pressure has shown an increase in the elastic constants and bulk moduli values [30] for rutile TiO_2. Moreover, the values of C_{11},C_{33}, C_{66}, C_{12} and C_{13} increase with increasing pressure whereas the pressure dependence of C_{44} is not clear. Moreover, the elastic constants are nonlinearly dependent on the temperature. Our *ab-initio* computational values of elastic constants and bulk moduli are fairly independent of any temperature and pressure variations to provide a reliable and independent set of values.

Another important area where the experiments are performed is the volume charge density and chemical bonding of rutile TiO_2. The quantitative convergent beam electron diffraction (QCBED) technique were employed by ref. [11] to determine the experimental volume charge density and chemical bonding. The experimental data was utilized to confirm the contribution of

ionic and covalent bonding in rutile TiO_2. The experimental charge density maps predicted the the $p-d$ hybridization between Ti 3-d electrons and O ligands.

The charge density influenced by highly localized d-orbitals of Ti atoms influences the selection of proper basis sets and potentials in *ab-initio* computations (see section on the potential, basis sets 1.2 and discussion of results 1.7).

Unlike the precision in the experimental lattice parameters, the computational values of lattice parameters vary in the second significant figures. The variation in the lattice parameter values is partially originated due to the complex nature of the chemical bonding of rutile TiO_2. Moreover, the sensitivity of the computational values of lattice parameters is attributed to the choice of potentials and basis sets. However, the hybrid potentials can map the chemical bonding and charge density of rutile TiO_2 with a considerable accuracy.

In general, the *ab-initio* computations are lacking the level of accuracy of the experiments. However, the extensive computational effort by refs. [7, 15, 1, 12, 6, 31] has provided guidance for the present study.

1.6. Computations

During the computations of lattice parameters and elastic properties, the SCF tolerances and other computational parameters were carefully chosen. The ELASTCON, EOS and SCF tolerances were adjusted due to the highly localized nature of transition metal Ti d-orbitals. The ELASTCON and other parameters were adjusted as $STEPSIZE$= 0.01, $NUMDERIV$= 7, $LGRID$ = (75, 434) and SHRINK= 9×9. The SCF tolerances were fixed as $TOLINTEG$=9 9 9 9 18 and $TOLDEE$= 9 [21].

1.7. Discussion of results

Tables 1 and 2 show the optimized lattice parameters computed with basis set 1 and 2, respectively. A considerable agreement between the computational and experimental values of lattice parameters computed with DFT-PWGGA, DFT-PBE, DFT-B3LYP and DFT-B3PW potentials can be seen in Table 1 refs. [2, 10, 4]. In contrast,the optimized lattice parameters deviate from the experimental values in case of basis set 2 as shown in Table 2.

Computational values of elastic constants and bulk moduli computed with ELASTCON are presented in Tables 3 and 4. For basis set 1, the agreement

between the computational and experimental values of elastic constants is better with non-local DFT and hybrid potentials only. The disagreement between the computational and experimental values of elastic constants is significantly higher for basis 2 as shown in Table 4. The values of elastic constants and bulk moduli are higher than the experimental values as O-6311d1 basis set fails to represent the chemical bonding required for rutile TiO_2.

Tables 5 and 6 show the comparisons between the bulk moduli values computed with ELASTCON and EOS algorithms. An excellent agreement is observed between the computational values of bulk moduli achieved with ELASTCON and EOS programs. The agreement between the bulk moduli values points at the computational accuracy of the ELASTCON and EOS programs. Moreover, it is important that a good agreement in computational results should also be crosschecked with the experimental values of the bulk moduli given at the bottom of Tables 5 and 6. Therefore, the Table 5 shows a better agreement between the computational and experimental values [4, 21, 1, 4, 5, 12].

However, there is a considerable disagreement between the computational and experimental values of C_{11}, C_{12}, C_{13}, C_{33}, C_{44}, C_{66} and B for basis set 1 and 2 with HF and DFT-LDA potentials as shown in Tables 3 and 4. On the other hand, the computational values of C_{11}, C_{12}, C_{13}, C_{33}, C_{44},C_{66} and B provide a significant agreement with the experimental values computed with DFT-PWGGA, DFT-PBE and hybrid potentials for basis set 1 as shown in Table 3.

In addition, a slightly better agreement between the computational and experimental values of lattice parameters, elastic constants and bulk moduli is observed for the hybrid potentials. The hybrid potentials have shown better agreement due to the adequate percentage of exchange and correlation contributions to total energy of the crystal specifically important due to the highly correlated physics of Ti transition metal. The localized nature of Ti atom d-orbitals contributes to the higher exchange and correlation effects.

The HF, local DFT and non-local DFT potentials can not predict as effectiveresults as hybrid potentials. Moreover, the computational values of lattice parameters, elastic constants and bulk moduli deviate from the corresponding experimental values for HF and DFT-LDA potentials [12, 6]. It can be easily seen in Tables 1, 2, 3, 4, 5 and 6. In fact, the lack of correlation in HF and localized nature of DFT-LDA potentials make these potentials less effective for transition metal oxides which possess the covalent

as well as ionic nature of chemical bonding.

It must be mentioned that DFT-PWGGA and DFT-PBE can predict better agreement with experimental results due to the non-localized nature of the rutile TiO_2 volume charge density. However, the agreement between the DFT-PWGGA, DFT-PBE and experimental results of elastic constants may not be adequate which can be confirmed by values in Tables 2, 4 and 6.

2. Part II: Computations On tetragonal $BaTiO_3$

The perovskites are an important class of materials with applications in the fields of memory, logic design and switching. However, the theoretical exploration of these materials is not on par with their technological importance. Crystalline $BaTiO_3$ possesses a perovskite geometry which may occur in cubic, tetragonal, rhombohedral or orthorhombic crystalline phases. There is a general lack of data on the mechanical properties of all phases of $BaTiO_3$. However, there have been attempts [32, 33, 34, 35, 36, 37, 38] to understand the electronic and mechanical properties of this material. For example, the computation of elastic constants and the bulk modulus was reported by Piskunov *et al* [39] for cubic $BaTiO_3$ using *ab-initio* computational methods. (See Fig. 7 for references)

At room temperature, $BaTiO_3$ has tetragonal crystalline geometry. In the past, the elastic constants and bulk modulus of tetragonal $BaTiO_3$ could not be computed due to the complexity of the system. Due to recent advancements in basis sets, geometry optimization, and computational power, *ab-initio* computational techniques can now be employed. In this paper, the computations of elastic constants and the bulk modulus of tetragonal $BaTiO_3$ are obtained with *ab-initio* Hartree Fock (HF), density functional theory (DFT) and hybrid potentials using two different basis sets.

An important factor that affects the efficiency and accuracy of computation is the determination of the optimized geometry of the crystalline structure. The geometry optimization is an essential step for calculating elastic constants and bulk moduli because it is assumed that all displacements are made relative to a system in equilibrium. The total geometry optimization finds both the atomic positions and lattice parameters of the unit cell which minimize the total energy. In addition, the geometry optimization in the CRYSTAL09 code [40] used here has features which make it an efficient program for calculating mechanical properties. For example, there is an option

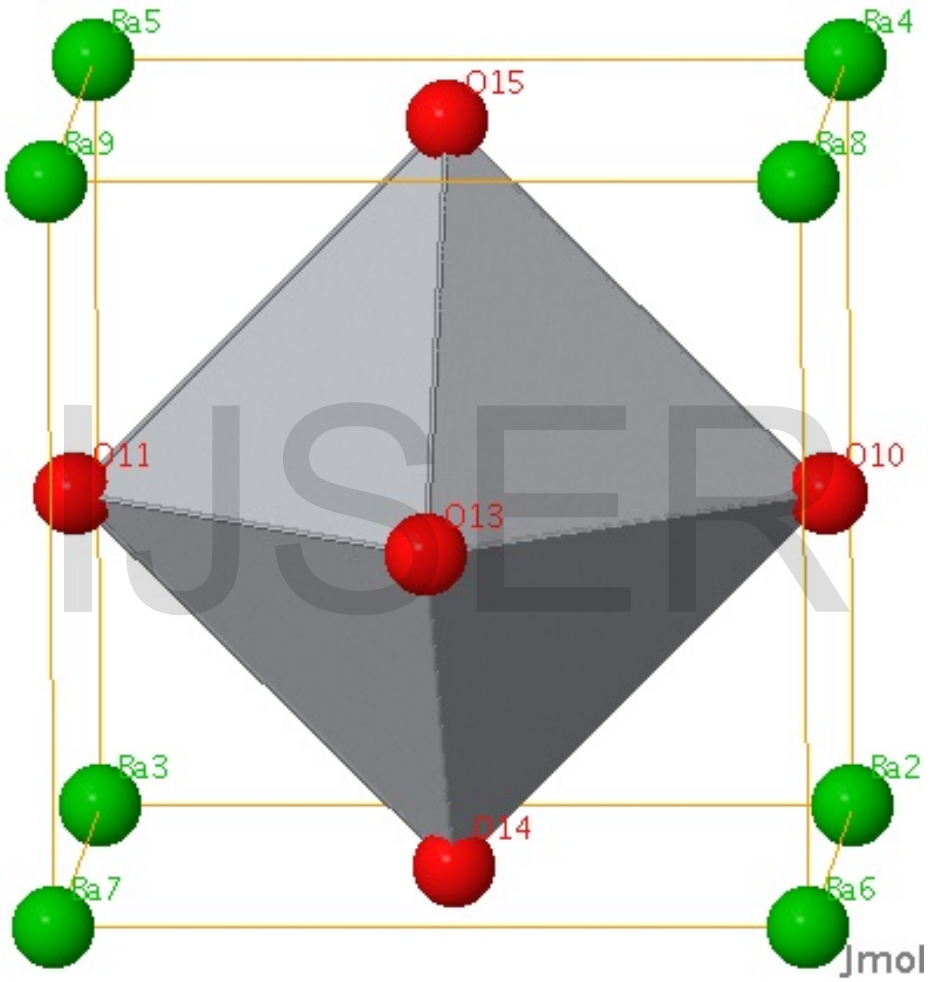

Figure 3: The The Unit Cell of tetragonal BaTiO3.

which permits optimization of the system at constant volume, which facilitates the determination of a total energy vs. volume curve which is necessary for equation of state (EOS) calculations.

As a cross-check, the bulk modulus is found independently with the program ELASTCON [**?**] and a separate EOS program. The ELASTCON algorithm determines the number of crystalline deformations based upon the crystalline geometry of tetragonal $BaTiO_3$. Geometry optimization of the crystalline structure is carried out after each deformation. The analytic first derivative, numerical second derivative and Levenberg Marquardt (LM) curve fitting is performed in sequence to compute elastic constants for the tetragonal $BaTiO_3$. A detailed discussion of the ELASTCON program can be found in refs. [**?** 44].

The task of crystalline geometry optimization of the perovskite $BaTiO_3$ has remained a challenge because the crystalline system undergoes a sudden decrease in energy when it is deformed. This sudden decrease in the strain vs. energy computations has been reported earlier [32, 41, 42] and was observed with the ELASTCON algorithm. Detailed energy vs. strain computations were carried out to explore this sudden decrease in energy.

2.1. Calculation of elastic constants with the CRYSTAL09 code

The computation of elastic constants and the bulk modulus is an automated process in the ELASTCON program. It begins with determining the crystalline symmetry of tetragonal $BaTiO_3$ and deformations are applied to exploit the available symmetries. The analytic first derivative and the numerical second derivative of total energy are computed for each deformation. Levenberg Marquardt (LM) curve fitting [24] is applied to compute the elastic constants. The computation of the elastic constants for tetragonal $BaTiO_3$ is complicated due to its crystalline geometry and the position of the atoms in the perovskite crystalline structure. With the lowering of crystalline symmetry, the number of independent elastic constants increases and geometry optimization steps are also increased.

The linear deformation of solids is expressed by Hooke's law as:

$$\sigma_{ij} = \sum_{kl} C_{ijkl}\epsilon_{kl} \tag{5}$$

where $i, j, k, l = 1, 2, 3$, $\sigma_{i,j,k,l}$, $\epsilon_{k,l}$ and $C_{i,j,k,l}$ are stress, strain and second-order elastic constant tensors.

The second-order elastic constants may be computed with different techniques. Molecular dynamics [43] and *ab-initio* computational techniques are two prominent methods to compute the elastic constants and bulk modulus. The *ab-initio* computational techniques compute the second-order elastic constant (SOEC) from the total energy. The elastic constants can be computed from the Taylor series expansion of the total energy with respect to the applied strains, as shown in Eq. (6). The Taylor series terms up to the second-order may be utilized for the estimation of the elastic constants if the strains are very small and the higher order terms have negligible effects on the computational results.

$$E\left(V,\epsilon\right) = E(V_0) + \sum_{\alpha} \sigma_\alpha \epsilon_\alpha + \frac{V}{2} \sum_{\alpha\beta} C_{\alpha\beta} \epsilon_\alpha \epsilon_\beta + ... \tag{6}$$

The terms $\alpha, \beta = 1, .., 6$ express the elastic constants in Voigt notation and V_0 is the equilibrium volume. The second term in Eq. (6) may be ignored if the crystalline geometry of the system is fully optimized. The third term in Eq. (6) can be rewritten to express the elastic constant as the second derivative of the total energy with respect to the applied strain in a crystalline direction

$$C_{\alpha\beta} = \frac{1}{V} \frac{\partial^2 E}{\partial \epsilon_\alpha \partial \epsilon_\beta}\bigg|_0. \tag{7}$$

In Eq. (7), the terms $C_{\alpha\beta}$, E, and V express the elastic constant tensor, energy and volume of the crystalline structure, respectively.

The *ab-initio* computations are achieved by calculating the analytic first derivative and numerical second derivative of the total energy with respect to the applied strain. The appropriate number of strains are applied in a systematic manner, the elastic constants are calculated, and the compliance coefficients are computed from Eq. (8). The compliance coefficients are then utilized for the computation of the bulk modulus as shown in Eq. (9).

$$[S] = [C]^{-1} \tag{8}$$

$$B = 1/(S_{11} + S_{22} + S_{33} + 2(S_{12} + S_{13} + S_{23})). \tag{9}$$

The terms S_{ij} and B in Eq. (9) express the compliance tensor elements and bulk modulus, respectively.

2.2. Computation of bulk modulus by equation of state (EOS)

The EOS algorithm utilizes systematic changes [44] in the volume around the optimized equilibrium state of a crystalline structure. The EOS calculations are carried out by selecting a range of volumes around a minimum total energy at an equilibrium state of the tetragonal $BaTiO_3$ crystalline structure. The EOS algorithm permits selection of a range of volumes and a number of volumes within that range. At each of the volumes in the range, the constant volume optimization is carried out. The energy vs. volume results are curve-fitted to an EOS such as Murnaghan EOS [25] given in Eq. (10).

The Crystal09 code [40] can accomplish an optimization of the internal co-ordinates and lattice parameters while keeping the volume constant (see ref. [40] for the detailed description of CVOLOPT option of geometry optimization). The EOS algorithm in CRYSTAL09 computes the energy for a range of volumes around the optimized equilibrium volume, and is equipped with a wide variety of equations of state such as Birch Murnaghan, 3rd order Birch Murnaghan, logarithmic, Vinet and polynomial. In this paper, the 3rd order Birch Murnaghan equation of state algorithm was utilized for computing the bulk modulus from the energy vs. volume computations as expressed in Eq. (10):

$$E(V) = B_o V_o \left[\frac{1}{B'(B'-1)} \left(\frac{V_o}{V} \right)^{B'-1} + \frac{V}{B'V_o} - \frac{1}{B'-1} \right] + E_o. \qquad (10)$$

In Eq. (10), V_0 represents the volume at the minimum energy, B_0 is the bulk modulus at pressure $P = 0$, $B^{'}$ is the derivative of the bulk modulus B at $P = 0$ and E_0 is the minimum energy. The optimization of crystalline geometry at each step is done during energy-volume (E-V) calculations. The bulk modulus results are obtained with Levenberg-Marquardt curve fitting of the E vs. V computations.

2.3. Choice of basis sets

The selection of basis sets affects the calculation of the elastic constants and bulk modulus as reported in refs. [45, 46, 6, 23], particularly for a material such as $BaTiO_3$. The first basis set chosen uses the 8-411d1 basis set for oxygen and HAYWSC ECP basis set for Ba and Ti atoms from the Crystal06 basis set library [40] because of its prior use in $BaTiO_3$ [39, 6]. For comparison, a second basis set, used previously for urea [45], was selected

using a 6-31d1 set for oxygen and the HAYWSC ECP for Ba and Ti. We have named the combination of basis sets 8-411d1 and HAYWSC ECP as basis set 1 and 6-31d1 and HAYWSC ECP as basis set 2.

As will be shown, the variation in the values of elastic constants and bulk modulus confirms the fact that the choice of basis sets can severely affect the results. The choice of basis sets indicates a trade-off between the reliability of the results and the required computational time. Our approach is to check the credibility of the results by employing the basis sets in two different algorithms for the bulk modulus and comparing the results attained using these basis sets with each other and experiment. In contrast with 6-31d1, the 8-411d1 basis set is optimized to suit the nature of chemical bonding and atomic position of oxygen in the transition metal oxide $ScMnO_3$ [23]. The positions of the oxygen atoms in $ScMnO_3$ is similar to a $BaTiO_3$ unit cell which has a slightly off-centered Ti atom caged in the middle of an octahderal formed by six oxygen atoms. Because of this, basis set 1 (with the 8-411d1 set for oxygen) is expected to provide better results for $BaTiO_3$.

2.4. Selection of Hartree Fock, DFT and hybrid potentials

The computations of elastic constants and the bulk modulus were performed with the potentials HF, DFT and hybrid mixing of the former with the latter. The DFT and hybrid exchange correlation potentials are employed due to the lack of correlation of HF as reported in [39].

In a hybrid potential, there is a significant balance between the electron exchange and correlation for a crystal field formed between the transition metal Ti and O nearest neighbors. Due to the effect of the crystal field, the transition metal oxides are insulators with a significantly higher band gap. This is unlike the situation in oxygen with s and p electrons resulting in an itinerant and delocalized electron gas. These d electrons are highly localized resulting in wide band gaps and a significant change in the probability density of inter-atomic and intra-atomic orbitals. The electron localization affects the choice of a basis set for oxygen atoms. It is very important that the basis set is optimized for the valence electrons of oxygen which are covalently bonded with a transition metal.

Corà [6] utilized HF, DFT and hybrid exchange correlation potentials and a 8-411d1 basis set for the oxygen atom of cubic $BaTiO_3$ to calculate the lattice constants, bulk modulus, and band gap. In that work, hybrid exchange and correlation potentials were used with an optimum percentage of HF exchange to account for the exchange and correlation parts of a highly

correlated transition metal oxide. Hybrid exchange correlation potentials were found to be efficient, reliable and accurate in comparison with HF and DFT potentials. Based on that prior work, hybrid exchange potentials are used here for the tetragonal phase of $BaTiO_3$.

2.5. Discussion of computational results

The comparison of lattice constants a, c and the ratio c/a with experimental values is shown in Tables 7 and 8 for basis sets 1 and 2, respectively. The values of optimized lattice constants have shown a better agreement with the experimental values for basis set 1 than basis set 2. The computational values of a and c are slightly higher than the experimental values for DFT-PWGGA, DFT-BLYP, DFT-B3LYP and DFT-B3PW exchange correlation potentials employed with basis set 1. The optimized lattice constants a and c computed with HF and DFT-LDA exchange correlation are included for reference but are not expected to produce good agreement with experiment because the HF potential has no correlation and the DFT-LDA assumes a homogeneous electron gas. Interestingly, the optimized values of lattice constants a and c computed with basis set 2 show relatively large deviations from the experimental values of 3.99 and 4.03. The values of the optimized lattice constants a and c are equal for Hartree Fock, exchange correlation and hybrid potentials employing basis set 2 as shown in Table 8. The fact that the tetragonal character has been missed for all potentials chosen suggests that basis set 2 is inadequate for this system. It is generally observed that local DFT (LDFT) exchange correlation potentials underestimate and non-local DFT (NLDFT) exchange correlation potentials overestimate the lattice constants.

The computational values of elastic constants and bulk moduli show a trend of better agreement with the experimental values for basis set 1 than for basis set 2 as shown in Tables 9 and 10. Likewise, the comparison of computational values of bulk moduli computed with the EOS method indicates a better agreement with experimental values as shown in Tables 11 and 12 for basis set 1 relative to basis set 2, respectively. Also given in those tables are the values of the bulk modulus determined from the ELASTCON calculation and the agreement in B using two, independent, methods demonstrates the quality of the numerical methods employed. The computational values of bulk moduli in Table 11 calculated with basis set 1, for DFT-BLYP, PWGGA, B3LYP and B3PW potentials, fall within the range of experimental values of

bulk modulus reported by [47]. The trend of consistency between the computational and experimental values of elastic constants and bulk moduli for basis set 1 vs. basis set 2 can also be seen by comparing results of elastic constants and bulk moduli shown in Figures 4-**??**. Comparing Figs. 4 and 5, it is evident that basis set 2 produces results for the bulk modulus consistently larger than experiment, whereas the basis set 1 results effectively bracket experiment. Those figures also show the good agreement between the two methods used to compute B. Fig. 6 using basis set 1 shows better agreement with experiment for the elastic constants than basis set 2 used in Fig. **??**, particularly for the hybrid potentials. Figs. 6 and **??** also indicate the spread in experimental values.

The discrepancy in results for lattice constants, elastic constants, and bulk modulus from basis set 2 and experiment [48, 49] is the consequence of the coefficients and exponents of the outermost Gaussian functions in a 6-31d1 basis set for the oxygen atom [45]. The 6-31d1 basis set was initially optimized for the oxygen atom in a unit cell of urea [45]. Therefore, the values of coefficients and exponents of these *sp* Gaussians are significantly larger to optimize the basis set for the requirements of hydrogen bonding and the peculiar position of the oxygen atom in a unit cell of urea[45, 46]. As a result, the values of elastic constants, particularly C_{11}, C_{33} and consequently bulk moduli (B), are largely affected by the values of these coefficients and exponents of *sp* type Gaussian functions. This is apparent from Table 10 where the values of C_{11} and C_{33} are consistently much larger than experiment and the results using basis set 1, Table 9. The basis sets are merely approximations of wavefunctions for valence electrons taking part in the chemical bonding. Therefore, the difference in the nature of chemical bonding in a urea vs. $BaTiO_3$ unit cell increases this inconsistency in the computational values for basis set 2 in comparison with basis set 1 and experimental values. The nature of chemical bonding is complex in $BaTiO_3$ and is different from the hydrogen bonding of urea. Moreover, the basis set 8-411d1 has already been optimized for *ab-initio* computations of magnetic properties of $ScMnO_3$ [23]. The transition metal oxide like $BaTiO_3$ is a highly correlated material system due to the contracted nature of its d orbitals. The localized nature of transition metal oxides demands an oxygen basis set which is specially optimized to suit these transition metal oxides as in refs. [6, 23, 39].

Regarding basis set 1, the DFT-LDA have shown higher bulk modulus values due to the underestimation of the optimized lattice constant values, whereas the computations done with DFT-PWGGA and DFT-BLYP have

shown lower values of bulk modulus due to the overestimation of optimized lattice constants. The computations done with hybrid potentials have shown the optimum values of bulk modulus as a consequence of the fact that the optimized lattice constants are comparatively close to the experimental values. In contrast with these results, the computational values of bulk modulus are higher with the basis set 2 as reported in Tables 11 and 12. The large increase in computational values of bulk modulus for the basis set 2 is attributed to the deviation in optimized lattice constants from the experimental values.

The computational results obtained with the PWGGA and hybrid potentials and basis set 1 are expected to be relatively accurate based on prior work for cubic $BaTiO_3$ [39] and rutile TiO_2 [**?**] crystalline systems. Moreover, the values of bulk modulus computed with ELASTCON and EOS algorithms are sufficiently close to each other for the same potential and basis set. These facts point to the importance of selecting a variety of basis sets, potentials and algorithms and comparing the results. Therefore, the computational values of elastic constants computed with hybrid potentials are reliable if we ignore the variations in computations originating due to the order-disorder nature of the tetragonal $BaTiO_3$.

While comparing the results of elastic constants and bulk moduli obtained with basis set 1 vs. experimental values and basis set 2 vs. experimental values, the former shows a relatively better agreement in comparison with the latter[50, 51, 52, 53, 47]. This agreement is specifically significant in the case of a hybrid exchange and correlation potential used with basis set 1. The computational accuracy of hybrid exchange and correlation potentials has been reported by Corà [6]. The computational values of bulk moduli of cubic $BaTiO_3$ are highly accurate for the optimum percentage of Hartree Fock and DFT exchange and DFT correlation potential. The accuracy of a hybrid exchange correlation potential is ingrained in the exchange and correlation parts of hybrid potential which improves the lattice parameters, bulk modulus and band gap of cubic $BaTiO_3$ as reported in ref. [6].

Regarding any comparisons made of computational to experimental values, it should be noted that for this system there is a considerable variation between the experimental values of elastic constants and bulk moduli [50, 51, 53, 47]. These variations in computational and experimental values of elastic constants and bulk moduli [50, 52, 54, 37, 47] have been constantly observed in a variety of experimental results. The causes of variation in experimental and computational values of elastic constants and bulk modulus may not be completely known. For the case of computational values, there

are significant contributions due to an inefficient basis set, as in case of basis set 2, which makes the choice basis set so vital for the accuracy of results. On the other hand, the variation in computational and experimental values may not be an isolated effect due to the effect of the crystalline geometry on the computational and experimental values.

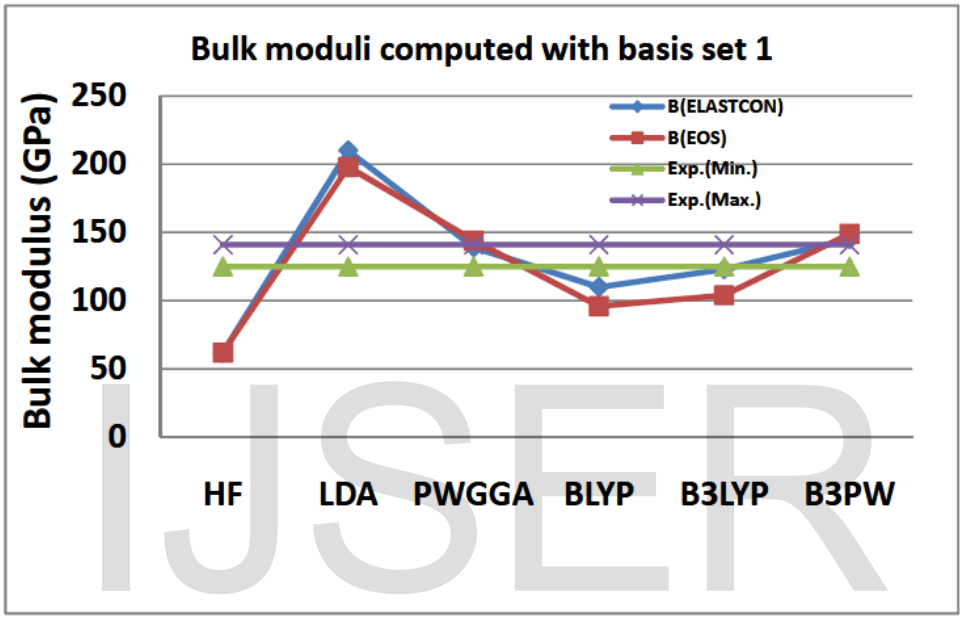

Figure 4: The computational values of bulk moduli are shown for basis set 1 computed with HF, DFT and hybrid functionals. The minimum and maximum experimental values of bulk moduli, titled as Exp.(Min.) and Exp.(Max.), are taken from ref. [47]. All values are in GPa.

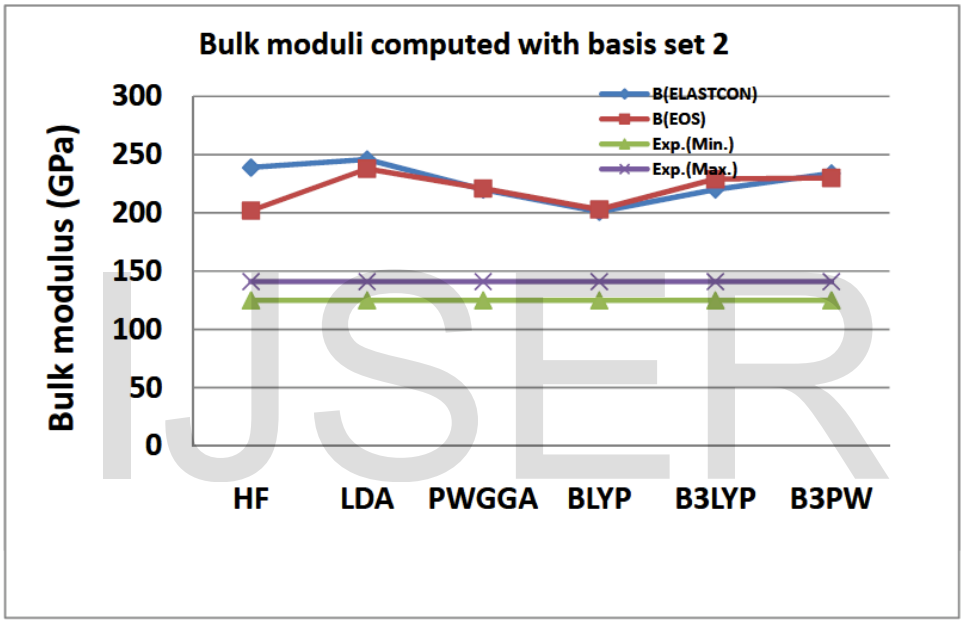

Figure 5: The computational values of bulk moduli are shown for basis set 2 computed with HF, DFT and hybrid functionals. The minimum and maximum experimental values of bulk moduli, titled as Exp.(Min.) and Exp.(Max.), are taken from ref. [47]. All values are in GPa.

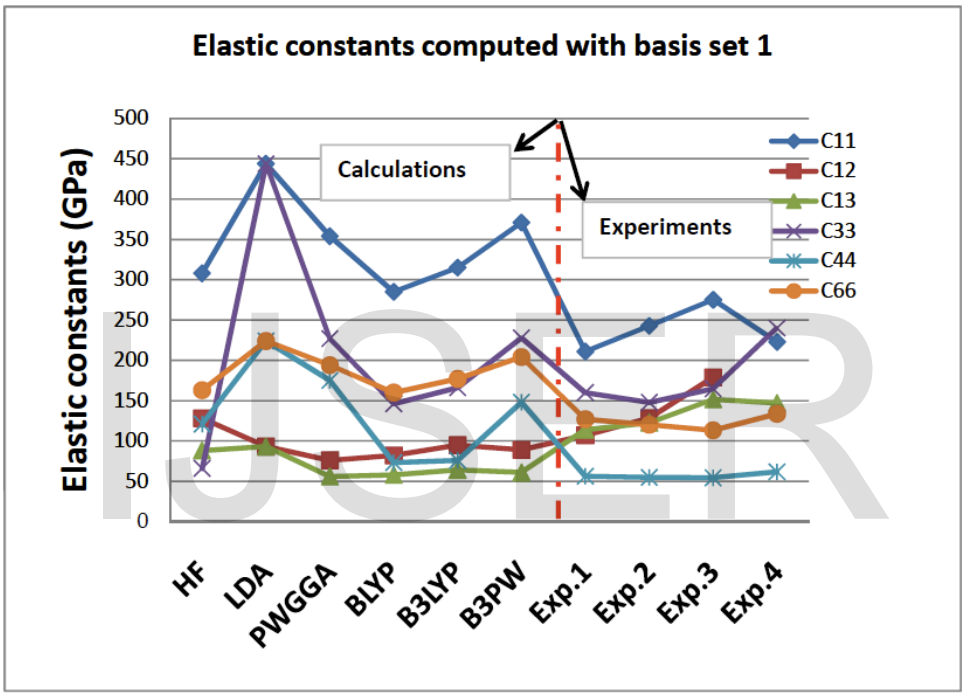

Figure 6: The computational and experimental values of elastic constants and bulk moduli are shown for basis set 1 computed with HF, DFT and hybrid exchange correlation potentials. The experimental values titled as Exp.1, Exp.2, Exp.3 and Exp.4 are taken from refs.[50, 51, 53, 52, 47]. All values are in GPa.

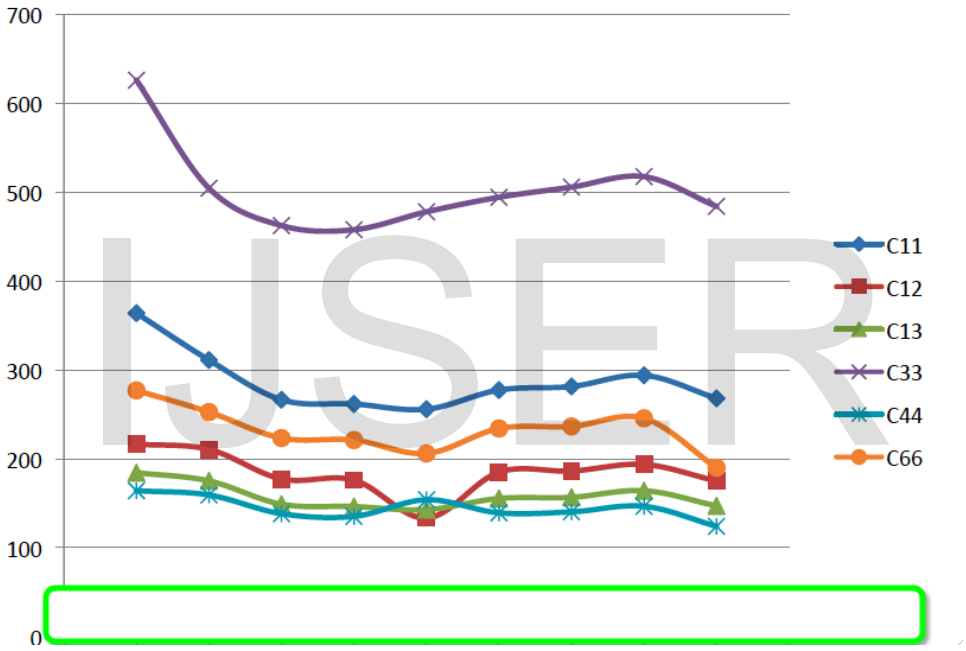

Figure 7: .

Table 1: **The values of relaxed lattice constants (in $\AA$) and ambient volume (in $\AA^3$) and total energy, E (in a.u.), for rutile TiO_2. Hartree-Fock, DFT exchange correlation and hybrid potentials were employed. Basis sets were selected from CRYSTAL09 basis set library [9]. (see sections 1.1, 1.2, 1.5 and 1.7 for details on the computational parameters, basis sets, potentials and analyses of results.)**

	$a(A^0)$	$c(A^0)$	$Vol.((A^o)^3))$	$Density(g/cm^3)$	$E(a.u.)$
HF	4.568	2.980	62.11	4.264	-415.125024
LDA	4.559	2.932	60.98	4.351	-415.4375020
PWGGA	4.640	2.976	64.08	4.140	-417.745101
PBE	4.647	2.978	64.32	4.125	-417.450436
BLYP	4.66	3.01	65.67	4.040	-417.646742
B3LYP	4.629	2.976	63.78	4.160	-417.525784
B3PW	4.599	2.961	62.63	4.236	-417.647585
PBE0	4.627	2.973	63.69	4.627	-417.800715
Exp.[2, 10, 4]	4.59	2.96	62.36	-	-

Table 2: **The values of relaxed lattice constants (in $\AA$) and ambient volume (in $\AA^3$) and total energy, E (in a.u.), for rutile TiO_2. Hartree-Fock, DFT exchange correlation and hybrid potentials were employed. Basis sets were selected from CRYSTAL09 basis set library [9]. (see sections 1.1, 1.2, 1.5 and 1.7 for details on the computational parameters, basis sets, potentials and analyses of results.)**

	$a(A^0)$	$c(A^0)$	$Vol.((A^o)^3))$	$Density(g/cm^3)$	$E(a.u.)$
HF	4.561	2.991	62.24	4.262	-415.030280
LDA	4.539	2.904	59.84	4.433	-4.15.303870
PWGGA	4.619	2.946	62.82	4.220	-417.622557
PBE	4.625	2.949	63.05	4.204	-417.329627
BLYP	4.657	2.971	64.41	4.117	-417.520930
PBE0	4.571	2.940	61.46	4.317	-417.245299
B3LYP	4.607	2.957	62.75	4.225	-417.408695
B3PW	4.583	2.942	61.81	4.292	-417.533064
Exp.[55]	4.593	2.958	62.40	-	-
Exp. [2, 10]	4.59	2.96	62.36	-	-

Table 3: **The values of elastic constants (in GPa) for rutile TiO_2. Hartree-Fock, DFT exchange correlation and hybrid potentials were used. Basis sets were selected from CRYSTAL09 basis set library [9]. All values are in GPa. (see sections 1.1, 1.2, 1.5 and 1.7 for details on the computational parameters, basis sets, potentials and analyses of results.)**

	C_{11}	C_{12}	C_{13}	C_{33}	C_{44}	C_{66}	B
HF	363.88	216.43	184.34	625.97	164.08	276.93	269.71
LDA	311.10	210.59	175.15	504.48	159.31	252.60	243.15
PWGGA	266.41	177.25	148.88	462.40	138.23	223.33	208.06
PBE	261.66	176.04	146.29	457.73	135.14	221.06	205.14
BLYP	255.76	133.27	142.78	477.90	153.90	206.05	187.60
PBE0	277.372	184.917	155.401	494.276	139.180	234.103	217.12
B3LYP	281.36	186.22	156.70	505.70	140.29	236.43	219.85
B3PW	293.89	193.64	164.11	517.48	146.55	245.56	229.13
Exp.[10]	268.00	175.00	147.00	484.00	124.00	190.00	212.00,230.00

Table 4: **The computational values of elastic constants and bulk moduli for rutile TiO_2. Hartree-Fock, DFT exchange correlation and hybrid potentials were employed. Basis sets were selected from CRYSTAL09 basis set library [9]. All values are in GPA. (see sections 1.1, 1.2, 1.5 and 1.7 for details on the computational parameters, basis sets, potentials and analyses of results.)**

	C_{11}	C_{12}	C_{13}	C_{33}	C_{44}	C_{66}	B
HF	393.38	237.08	209.69	662.10	170.85	302.60	295.27
LDA	170.95	384.96	204.67	577.12	130.39	278.53	265.91
PWGGA	222.60	273.01	182.34	522.34	123.35	246.21	237.24
PBE	220.46	269.67	180.65	517.01	122.22	243.67	234.72
BLYP	259.83	225.99	174.58	508.73	123.33	235.50	231.32
PBE0	267.06	281.97	203.06	578.72	138.82	-	-
B3LYP	295.27	239.63	192.98	562.44	137.12	261.30	254.96
B3PW	268.97	269.36	197.01	568.79	136.54	267.48	257.44
Exp.[10]	268.00	175.00	147.00	484.00	124.00	190.00	212.00,230.00

Table 5: **Equation of state (EOS) computations of bulk moduli for rutile TiO_2. Hartree-Fock, DFT exchange correlation potentials and hybrid potentials were employed. Basis sets were selected from CRYSTAL09 basis set library [9]. (see sections 1.1, 1.2, 1.5 and 1.7 for details on the computational parameters, basis sets, potentials and analyses of results.)**

	B_{EOS}(GPa)	$V_o(\AA^3)$	$E_0(a.u.)$	B_{EL}(GPa)
LDA	241.02	60.98	-415.4374458	243.15
PWGGA	205.84	64.09	-417.745066	208.06
PBE	202.42	64.33	-417.450408	205.14
BLYP	190.81	65.93	-417.646784	187.60
B3LYP	216.58	63.81	-417.525805	219.85
B3PW	226.04	62.66	-417.647557	229.13
HF	266.65	62.29	-415.125014	269.71
Exp.[10]	-	-	-	212.00,230.00

Table 6: **Equation of state (EOS) computations of bulk moduli for rutile TiO_2. Hartree-Fock, DFT exchange correlation potentials and hybrid potentials were employed. Basis sets were selected from CRYSTAL09 basis set library [9]. (see sections 1.1, 1.2, 1.5 and 1.7 for details on the computational parameters, basis sets, potentials and analysis of results.)**

	B_{EOS}(GPa)	$V_o(\AA^3)$	$E_0(a.u.)$	B_{EL}(GPa)
HF	292.73	62.31	-415.030267	295.27
LDA	278.99	59.84	-415.303858	282.68
PWGGA	238.71	62.87	-417.622543	237.24
PBE	235.96	63.10	-417.329611	234.72
BLYP	229.03	64.45	-417.520911	231.32
B3LYP	252.43	62.81	-417.408677	254.96
B3PW	256.16	61.83	-417.533045	257.44
Exp.[10]	-	-	-	212.00,230.00

Table 7: **The values of relaxed lattice constants (in $\AA$), ambient volume (in $\AA^3$), and total energy, E (in a.u.), for tetragonal $BaTiO_3$. The computations were done by using Hartree-Fock, DFT LDA, PWGGA, BLYP, B3LYP and B3PW potentials using basis set 1. (see section 2.3).**

	a	c	c/a	Vol.	E
HF	3.96	4.26	1.07	67.17	-307.5388
LDA	3.93	3.93	1.00	61.12	-307.8828
PWGGA	4.00	4.03	1.00	64.75	-309.5928
BLYP	4.05	4.14	1.02	68.12	-309.4749
B3LYP	4.01	4.10	1.02	66.15	-309.4084
B3PW	3.98	4.02	1.01	63.75	-309.5360
Exp. [48, 49]	3.99	4.03	1.01	64.16	-

Table 8: **The values of relaxed lattice constants (in$\AA$), ambient volume (in $\AA^3$), and total energy, E (in a.u.), for tetragonal $BaTiO_3$. The lattice constants are computed with Hartree-Fock, DFT LDA, PWGGA, BLYP, B3LYP and B3PW potentials with basis set 2 (see section 2.3). O-631d1 basis set for O atom was not optimized for transition metal oxides resulting in the lattice parameters that differ significantly from experimental values.**

	a	c	c/a	Vol.	E
HF	3.98	3.98	1.00	63.23	-307.4627
LDA	3.90	3.90	1.00	59.50	-3.07.7595
PWGGA	3.95	3.95	1.00	61.94	-309.4862
BLYP	4.00	4.00	1.00	64.06	-309.3636
B3LYP	3.97	3.97	1.00	62.66	-309.3082
B3PW	3.94	3.94	1.00	61.27	-309.4393
Exp. [48, 49]	3.99	4.03	1.01	64.16	-

Table 9: **The elastic constants and bulk modulus computational results using the Hartree Fock and DFT LDA, PWGGA, BLYP, B3LYP and B3PW potentials with basis set 1 (see section 2.3). All values are in GPa.**

	C_{11}	C_{12}	C_{13}	C_{33}	C_{44}	C_{66}	B
HF	308.	128.	88.	66.	121.	163.	62.
LDA	444.	93.	93.	444.	224.	224.	210.
PWGGA	354.	76.	56.	227.	175.	194.	139.
BLYP	285.	82.	58.	146.	73.	160.	110.
B3LYP	315.	95.	64.	166.	76.	177.	123.
B3PW	371.	89.	61.	228.	148.	204.	145.
Exp.[50]	211±6	107±5	114±8	160 ±11	56.2±1.7	127±4	125-141[47]
[51]	242.7	128.3	122.6	147.9	54.9	120.1	-
[53]	275.1	178.9	151.55	164.8	54.3	113.1	-
[52]	222.9	-	147.0	240.0	61.7	133.7	-

Table 10: **The elastic constants and bulk modulus computations using the Hartree Fock, DFT LDA, PWGGA, BLYP, B3LYP and B3PW potentials with basis set 2 (see section 2.3). All values are in GPa.**

	C_{11}	C_{12}	C_{13}	C_{33}	C_{44}	C_{66}	B
HF	408.	154.	154.	408.	185.	185.	239.
LDA	480.	129.	129.	480.	163.	163.	246.
PWGGA	445.	107.	107.	445.	214.	214.	220.
BLYP	382.	111.	111.	382.	185.	185.	201.
B3LYP	414.	123.	123.	414.	200.	200.	220.
B3PW	463.	119.	119.	463.	223.	223.	234.
Exp.[50]	211±6	107±5	114±8	160 ±11	56.2±1.7	127±4	125-141[47]
[51]	242.7	128.3	122.6	147.9	54.9	120.1	-
[53]	275.1	178.9	151.55	164.8	54.3	113.1	-
[52]	222.9	-	147.0	240.0	61.7	133.7	-

Table 11: **Equation of state results for tetragonal $BaTiO_3$ with the Birch Murnaghan 3rd order equation. The energy-volume curve was fitted with eleven points and the range of volume around equilibrium was chosen as ±10% using basis set 1 (see section 2.3). The value of the bulk modulus, B_{EL}, as calculated from Eq. (9) is given in the last column for comparison.**

	B_{EOS}(GPa)	$V_o(\mathring{A}^3)$	$E_0(a.u.)$	B_{EL}(GPa)
HF	62.	67.41	-307.5386	62.
LDA	198.	61.16	-307.8827	210.
PWGGA	144.	64.75	-309.5928	139.
BLYP	96.	68.09	-309.4749	110.
B3LYP	104.	66.07	-309.4083	123.
B3PW	149.	63.82	-309.5360	145.
Exp.[47]	125-141	-	-	

Table 12: **Equation of state data for $BaTiO_3$ using the 3rd-order Birch Murnaghan equation. Eleven points in the energy-volume curve were used and the range of volumes used around equilibrium was ±10% using basis set 2 (see section 2.3). The value of the bulk modulus, B_{EL}, as calculated from Eq. (9) is given in the last column for comparison.**

	B_{EOS}(GPa)	$V_o(\mathring{A}^3)$	$E_0(a.u.)$	B_{EL}(GPa)
HF	202.	64.23	-307.4678	239.
LDA	238.	59.07	-307.7672	246.
PWGGA	221.	61.93	-309.4862	220.
BLYP	203.	64.09	-309.3636	201.
B3LYP	229.	62.77	-309.3082	220.
B3PW	230.	61.41	-309.4395	234.
Exp. [47]	125-141	-	-	

3. Part III: Conclusions

3.1. Rutile Titanium dioxide (TiO_2)

The technological applications of Titanium dioxide (TiO_2) have generated a significant research activity in experimental and computational sciences. The advantages of the experimental and computational research has resulted in an enhancement in testing the merit of basis sets, potentials and new programs. The elastic properties of rutile TiO_2 are computed and compared

with experimental values. The dependance of experimental values on experimental set up, temperature and pressure conditions can not be ignored. The computations of elastic constants and bulk moduli by a wide variety of *ab-initio* techniques provide results to generate fresh experiments on this material.

We have tried to separate the factors that determine the quality of computational results of the lattice parameters and elastic properties. The non-local DFT and hybrid potentials present better agreement with the experimental values of lattice parameters, elastic constants and bulk moduli. However, the disagreement between the computational and experimental values of the elastic constants and bulk moduli for HF and DFT-LDA potentials [16, 17, 19] is quite significant.

It is worth mentioning that computations of rutile TiO_2 with different potentials and basis sets is motivated by a variety of challenges related with the existing basis sets and potentials. For a crystalline system such as rutile TiO_2, which has considerable visibility in the experimental research arena, an intergrated set of computational results have significant utility. These computations can guide researchers to appreciate the subtle influcences of the charge density on lattice parameters and elastic properties of rutile TiO_2.

3.2. Tetragonal $BaTiO_3$

The second order elastic constants and equations of state parameters were obtained for tetragonal $BaTiO_3$. We have observed close agreement between the values of the bulk modulus independently computed with ELASTCON and EOS methods. There have been attempts [56, 57, 58] to compute the different properties of tetragonal $BaTiO_3$. However, the computational values of elastic constants and bulk modulus of tetragonal $BaTiO_3$ are not available in the literature. We have further verified the computational accuracy of the results by implementing different algorithms, potentials and basis sets for rutile TiO_2 [**?**] and cubic $BaTiO_3$ [39]. The computational results obtained with these crystalline systems have provided additional evidence for the accuracy of the computational results presented here for tetragonal $BaTiO_3$. It has been observed that the crystalline structure and position of atoms in tetragonal phase [59, 60] has increased the complexity of our computations. The agreement in computational values of bulk modulus provided an opportunity to verify the computational accuracy of elastic constants of tetragonal $BaTiO_3$.

The computational results of the optimized lattice constants obtained with basis set 1 and exchange correlation potential PWGGA and hybrid exchange correlation potentials B3LYP and B3PW have shown good agreement with respect to experiment. Therefore the employment of HF, DFT and hybrid exchange correlation potentials have essentially reinforced the computational merit of hybrid potentials as was found by Corà [6] for cubic phase $BaTiO_3$. The variations in computational values of elastic constants and bulk moduli are mainly attributed to the quality of basis sets and choice of potential. Basis set 1 is better designed to represent the interatomic and intra-atomic chemical nature of O, Ti and Ba for $BaTiO_3$ and, as expected, provided better agreement with experiment than basis set 2. It is important to note that differences in the *sp* orbital basis set for oxygen resulted in large differences in the C_{11} and C_{33} elastic constants. The inconsistency in computational results of elastic constants and bulk modulus for the two chosen basis sets compared with experimental values points at the importance of choosing an appropriate basis set for reliable and accurate *ab-initio* computations.

The order -disorder nature [60] of perovskite $BaTiO_3$ is another important factor that makes the computation of optimum values of the bulk modulus problematic, requiring accurate basis sets and potentials. It has been observed that the computation of the bulk modulus for tetragonal $BaTiO_3$ is coupled intimately with the geometry optimization of its complex crystalline structure. Slight deviations in the values of optimized lattice constants a and c have shown large effects on the computational values of bulk moduli.

Based upon our computational results and the experimental data on tetragonal $BaTiO_3$, we conclude that there is a degree of consistency in the elastic properties. Further work on basis sets and exchange correlation potentials is necessary for improved comparison with experiment. Additionally, improvements in the experiments are important for continued progress on this important crystalline system.

A close look at the computational results of the Rutile TiO2 and tetragonal BaTiO3 reveals the anomaly in the elasticity of the tetragonal BaTiO3. The anomaly is highly pronounced in some crystal directions and less pronounced in other directions. It took us costly computations of Rutile TiO2 to expose and reveal the complexity of tetragonal BaTiO3 phase. The novel extraction has been reported by us for the first time through the complex computational formalism.

[1] F. Labat, P. Baranek, C. Domain, C. Minot, C. Adamo, The Journal of Chemical Physics 126 (2007) 1–12.

[2] S. Tanemuraa, L. Miaoa, W. Wunderlicha, M. Tanemuraa, Y. Morib, S. Tohc, K. Kanekoc, Science and Technology of Advanced Materials 6 (2005) 11–17.

[3] M. Shang-Di, C. W. Y., Phys. Rev. B (1995) 13023.

[4] H. Yao, L. Ouyang, W.-Y. Ching, J. Am. Ceram. Soc. (2007) 3194–3204.

[5] B. D. I., O. R., S. R., R. G.-M., J. Íñiguez, G. Ph., Phys. Rev. B 77 (2008) 165107.

[6] F. Corà, Molecular Physics (2005) 2483–2496.

[7] C. Adamo, V. Barone, J Chem Phys 110 (1999) 6158–6170.

[8] M. E. Stizaumainis, T. Ejima, W. J. James, Acta Cryst. 8 (1961) 493–97.

[9] R. Dovesi, V. R. Saunders, C. Roetti, R. Orlando, C. M. Zicovich-Wilson, F. Pascale, B. Civalleri, K. Doll, N. M. Harrison, I. J. Bush, P. D'Arco, M. Llunell, *CRYSTAL2006* User's Manual, University of Torino, University of Torino, Torino, Italy, 2006.

[10] M. Iuga, G. Steinle-Neumann, J. Meinhardt, Eur. Phys. J. B 58 (2007) 127–133.

[11] J. B., Z. J. M., J. N., O. M., S. J. C. H., Acta Cryst. (2003) 341.

[12] C. Furio, A. Maria, M. Giuseppe, M. Derek, M. William, D. Roberto, O. Roberto, Principles and Applications of Density Functional Theory in Inorganic Chemistry II (2004) 171.

[13] W. F. Perger, J. Criswell, B. Civalleri, R. Dovesi, *ab-initio* calculation of elastic constants of crystalline systems with the CRYSTAL code, Comput. Phy. Comm. (2009) 1753–1759.

[14] B. H. OĆonnor, S. Pratapa, Advances in X-ray Analysis 45 (2002) 158–165.

[15] F. Labat, P. Baranek, C. Adamo, J. Chem. Theory Comput. 4 (2008) 341–352.

[16] M. Mikami, S. Nakamura, O. Kitao, H. Arakawa, X. Gonze, Jpn. J. Appl. Phys. 39 (2000) L847–L850.

[17] X. Ma, P. Liang, L. Miao, S. Bie, C. Zhang, L. Xu, J. Jiang, H. Yao, L. Ouyang, W. Ching, Phys. Status Solidi B (2009) 2132–2139.

[18] Y. Liu, L. Ni, Z. Ren, G. Xu, C. Song, G. Han, J. Phys. Condens. Matter 21 (2009) 275901–6.

[19] N. M. H. Joseph Muscat Varghese Swamy, Phys. Rev. B (2010) 224112.

[20] E. Shojaee, M. R. Mohammadizadeh, J. Phys. Condens. Matter 22 (2010) 1–8.

[21] Z. J.-Z. G.-T. L. Yong-Cheng, Chin. Phys. Lett. 25 (2008) 4356–59.

[22] G. Francois, K. Winfried, Phys. Rev. B 31 (1985) 4809–4814.

[23] T. Bredow, K. Jug, R. A. Evarestov, Phys. Stat. Sol. (2006) R10–R12.

[24] W. Marquardt, SIAM J. Appl. Math. 11 (1963) 431–44.

[25] F. D. Murnaghan, Proc. Natl. Acad. Sci. (USA) 30(9) (1944) 244–7.

[26] I. J. Fritz, Journal of Physics and Chemistry of Solids 35 (1974) 817–826.

[27] H. R. F. S., Rev. Mod. Phys. 18 (1946) 409–440.

[28] L. Gerward, J. S. Olsen, J. Appl. Cryst. 30 (1997) 259–264.

[29] L. Kóci, D. Y. Kim, J. S. D. Almeida, M. M. E. Isaev, R. Ahuja, J. Phys. Condens. Matter (2008) 345218.

[30] Z. Jun, Y. JingXin, W. YanJu, C. XiangRong, J. FuQian, Chin. Phys. Soc. 17 (2008) 2216–21.

[31] H. K., A. V., V. Eyert, K. G., M. A., N. I., V. D., Lda+dmft investigations of transition metal oxides and f-electron materials, in: Advances in Solid State Physics, Vol. 43 of Advances in Solid State Physics, Springer Berlin / Heidelberg, 2003, pp. 267–286.

[32] P. Ghosez, First-principles study of the dielectric and dynamic properties of Barium Titanate, Universite catholique De Louvain, Faculte des Sciences Appliques, 1997.

[33] A. Bouhemadou, K. Haddadi, Solid State Sciences (2010) 630–36.

[34] J. D. Freire, R. S. Katiyar, Phy. Rev. B (1988) 2074–85.

[35] J. Kung, R. A. Angel, N. L. Ross, Phys. Chem. Minerals (2001) 35–43.

[36] N. Orlovskaya, K. Kleveland, T. Grande, M. .-A. Einarsrud, Jrnl. European Cera. Soc. (1991) 50–56.

[37] T. Ishidate, S. Abe, H. Takahashi, N. Mori, Phy. Rev. Lett. (1997) 2397–2400.

[38] E. V. Mejia-Uriarte, R. Y. Sato-Berru, M. Navarrete, M. Villagran-Muniz, C., Medina-Guerrez, C. Frausto-Reyes, H. Murrieta, Meas. Sci. Technol. (2006) 1319–23.

[39] S. Piskunov, E. Heifets, R. I. Eglitis, G. Borstel, Bulk properties and electronic structure of $SrTiO_3$, $BaTiO_3$, $PbTiO_3$ perovskites: An *ab initio* HF/DFT study, Comput. Mater. Sci. (2004) 165–178.

[40] R. Dovesi, V. R. Saunders, C. Roetti, R. Orlando, C. M. Zicovich-Wilson, F. Pascale, B. Civalleri, K. Doll, N. M. Harrison, I. J. Bush, P. D'Arco, M. Llunell, *CRYSTAL2006* User's Manual, University of Torino, University of Torino, Torino, Italy, 2006.

[41] M. Uludogan, T. Cagin, W. A. Goddard MRS web archive.

[42] H. Salehi, S. M. Hosseini, N. Shahtahmasebi, Chin. J. Phys. 42 (2004) 619–27.

[43] A. Khalal, D. Khatib, B. Jannot, Physica B (1999) 343–47.

[44] W. F. Perger, Int. J. Quant. Chem. (2010) 1916–1922.

[45] C. Gatti, V. R. Saunders, C. Roettti, J. Chem. Phys. (1994) 10686–96.

[46] A. Shukla, E. D. Isaacs, D. R. Hamann, P. M. Platzman, Phy. Rev. B (2001) (052101)–1–4.

[47] L. Feng-Ying, J. Chang-Qing, Y. Shu-Jie, X. Chang-Jiang, Y. R. Cheng, W. Xiao-Hui, L. Jing, L. Xiao-Dong, L. Yan-Chun, C. Liang-Chen, Chin. Phy. Lett. (2006) 1249–52.

[48] J. Donohue, S. J. Miller, R. F. Cline, Acta. Cryst. 11 (1958) 693–695.

[49] U. A. Joshi, S. Yoon, S. Baik, J. S. Lee, J. Phys. Chem. B 110 (2006) 12249–56.

[50] Z. Li, S. K. Chan, M. H. Grimsditch, E. S. Zouboulis, J. Appl. Phys. (1991) 7327–32.

[51] A. Schaefer, H. Schmitt, A. Dorr, Ferroelectrics (1986) 253–66.

[52] T. Ishidate, S. Sasaki, J. Phys. Sot. Jpn. (1987) 4214–17.

[53] D. Berlincourt, H. Jaffe, Phys. Rev. (1958) 353–266.

[54] T. Ishidate, S. Sasaki, Phys. Rev. Lett. (1989) 67–70.

[55] J. K. Burdett, T. Hughbanks, G. J. Miller, J. W. Richardson, J. V. Smith, J. Am. Chem. Soc. 109.

[56] A. C. Dent, C. R. Bowen, R. Stevens, M. G. Cain, M. Stewart, Eur. Ceram. Soc. J. 27 (2007) 3739–43.

[57] W. C. Mei, D. Y. Feng, C. C. Qing, Chin. Phys. L. 26 (2009) (017203)–1–4.

[58] R. S. Kumar, A. L. Cornelius, M. F. Nicol, Phys. Stat. Sol. 244 (2006) 290–294.

[59] G. H. Kwei, A. C. Lawson, S. J. L. Billinge, S. W. Cbeong, J. Phys. Chem. 97 (1993) 2368–77.

[60] R. Blinc, Springer Berlin/Heidelberg 124 (2007) 51–67.